


The RNA-Binding Protein HuR Is Integral to the Function of Nociceptors in Mice and Humans

Nikesh Kunder,^{1*} June Bryan de la Peña,^{2*} Tzu-Fang Lou,¹  Rebecca Chase,¹ Prarthana Suresh,¹ Jennifer Lawson,³ Tarjani Shukla,² Bryan Black,³ and Zachary T. Campbell^{2,4}

¹Department of Biological Sciences, University of Texas at Dallas, Richardson, Texas 75080, ²Department of Anesthesiology, School of Medicine and Public Health, University of Wisconsin–Madison, Madison, Wisconsin 53792, ³Department of Biomedical Engineering, University of Massachusetts Lowell, Lowell, Massachusetts 01854, and ⁴Department of Biomolecular Chemistry, School of Medicine and Public Health, University of Wisconsin–Madison, Madison, Wisconsin 53792

HuR is an RNA-binding protein implicated in RNA processing, stability, and translation. Previously, we examined protein synthesis in dorsal root ganglion (DRG) neurons treated with inflammatory mediators using ribosome profiling. We found that the HuR consensus binding element was enriched in transcripts with elevated translation. HuR is expressed in the soma of nociceptors and their axons. Pharmacologic inhibition of HuR with the small molecule CMLD-2 reduced the activity of mouse and human sensory neurons. Peripheral administration of CMLD-2 in the paw or genetic elimination of HuR from sensory neurons diminished behavioral responses associated with NGF- and IL-6-induced allodynia in male and female mice. Genetic disruption of HuR altered the proximity of mRNA decay factors near a key neurotrophic factor (TrkA). Collectively, the data suggest that HuR is required for local control of mRNA stability and reveals a new biological function for a broadly conserved post-transcriptional regulatory factor.

Key words: mRNA; nociceptor; pain; plasticity; RNA-binding; translation

Significance Statement

Nociceptors undergo long-lived changes in excitability, which may contribute to chronic pain. Noxious cues that promote pain lead to rapid induction of protein synthesis. The underlying mechanisms that confer specificity to mRNA control in nociceptors are unclear. Here, we identify a conserved RNA-binding protein called HuR as a key regulatory factor in sensory neurons. Using a combination of genetics and pharmacology, we demonstrate that HuR is required for signaling in nociceptors. In doing so, we report an important mechanism of mRNA control in sensory neurons that ensures appropriate nociceptive responses to inflammatory mediators.

Introduction

Post-transcriptional regulation of mRNA permeates neuronal plasticity (Wang and Tiedge, 2004; Costa-Mattioli et al., 2009). mRNAs possess two untranslated regions (UTRs) on opposing ends of the transcript. UTRs serve critical functions as repositories of information that is encoded by specific sequences and

structural elements. RNA-binding proteins and regulatory RNAs decode this information to enact precise control of mRNA export, localization, translation, and stability. The biological functions of RNA-binding proteins are pervasive. Their roles in pain associated plasticity are increasingly expansive (Price et al., 2007; Bogen et al., 2012; Sanna et al., 2015; Fong et al., 2016; Iida et al., 2016; Moy et al., 2017; Sanna et al., 2017; Barragán-Iglesias et al., 2018; de la Peña and Campbell, 2018; Loerch et al., 2018; de la Peña et al., 2019; Borgonetti and Galeotti, 2021; Chase et al., 2022).

HuR is a paradigmatic RNA-binding protein. It was discovered in *Drosophila* and designated embryonic lethal abnormal vision (ELAV; Hinman and Lou, 2008). In mammals, it has been implicated in a broad array of biological functions that span immunity, neurodegeneration, neurogenesis, and microglial activation following nerve injury (Diaz-Muñoz et al., 2015; Skliris et al., 2015; Borgonetti and Galeotti, 2021; Osmá-García et al., 2021). HuR governs the cytoplasmic fate of specific transcripts (Srikantan and Gorospe, 2012). It binds to AU-rich elements situated primarily in 3'UTRs. It generally promotes translation and

Received Aug. 26, 2022; revised Oct. 4, 2022; accepted Oct. 12, 2022.

Author contributions: N.K., J.B.D., B.B., and Z.T.C. designed research; N.K., J.D., T.-F.L., R.C., P.S., J.L., T.S., and B.B. performed research; N.K., J.B.D., T.-F.L., R.C., and T.S. analyzed data; and N.K., J.B.D., and Z.T.C. wrote the paper.

This work was supported by National Institutes of Health–National Institute of Neurological Disorders and Stroke Grants R01NS100788 (Z.T.C.) and R01NS114018 (Z.T.C.) and National Institutes of Health–National Center for Advancing Translational Sciences Grant 1UG3TR003149 (B.B.). CMLD-2 was obtained from Jeffrey Aubé from the University of North Carolina at Chapel Hill by a materials transfer agreement with the University of Texas at Dallas.

*N.K. and J.B.D. contributed equally to this work.

The authors declare no competing financial interests.

Correspondence should be addressed to Zachary T. Campbell at zcampbell@wisc.edu.

<https://doi.org/10.1523/JNEUROSCI.1630-22.2022>

Copyright © 2022 the authors

mRNA stability (López De Silanes et al., 2004; Lebedeva et al., 2011; Mukherjee et al., 2011). Multiple mechanisms have been reported to account for the regulatory effects of HuR. They include modulation of miRNA-mediated repression, epigenetic editing of transcripts, and regulated changes in shuttling between the nucleus and the cytoplasm (Abdelmohsen et al., 2007; Hyeon et al., 2009; Lafarga et al., 2009; Masuda et al., 2011; Filippova et al., 2012; Al-Khalaf and Aboussekhra, 2014; Wang et al., 2014). HuR is present in neurons and accumulates in dendrites following seizure or cocaine treatment (Tiruchinapalli et al., 2008). It associates physically with specific transmembrane receptors linked to activity-dependent protein synthesis (Koppers et al., 2019). An unresolved question is whether HuR plays a major role in local translation.

Inflammatory mediators have profound effects on nascent translation. Interleukin-6 (IL-6) and nerve growth factor (NGF) are integral to inflammation-associated pain in humans and rodents (Melemedjian et al., 2010; Barker et al., 2020; Sebba, 2021). Peripheral administration of either is sufficient to induce pain-associated behaviors (Melemedjian et al., 2010). Pharmacologic inhibition of translation blocks pain amplification by both mediators. Mechanistically, NGF and IL-6 increase translation and stimulate the mammalian target of rapamycin (mTOR) and mitogen-activated protein kinase (MAPK) pathways, albeit to slightly different degrees (Melemedjian et al., 2010). We recently applied ribosome profiling to primary DRG neurons treated with NGF and IL-6 for 20 min (de la Peña et al., 2021a). Among the hundreds of mRNAs with increased ribosome density were Arc and Fos, two immediate early genes implicated in plasticity (Bullitt, 1990; Lyford et al., 1995; Steward et al., 1998; Zhang et al., 2006; Minatohara et al., 2015). Their induction hinges on the activity of the downstream mTOR target ribosomal protein S6 kinase 1 (de la Peña et al., 2021b). These results provide a glimpse into the mechanisms that underlie induced translation in sensory neurons. Yet, it is unclear if information present in UTRs shapes the translational response to inflammatory mediators.

We examined our prior ribosome profiling data for enrichment of motifs in the 3' UTR of preferentially translated mRNAs (de la Peña et al., 2021a). We focus on this region given its pervasive involvement in the specification of mRNA fate. We found enrichment of a U-rich element. Parallel efforts revealed the binding specificity of HuR using an unbiased functional genomics approach. HuR binding elements are enriched in mRNAs whose translation is increased by NGF and IL-6. HuR is expressed in most populations of DRG neurons and is present in the soma and axons of nociceptors. Pharmacologic inhibition of HuR decreased firing of mouse DRG or human stem-cell-derived sensory neurons. Deletion of HuR from sensory neurons blocked acute and persistent changes in mechanical hypersensitivity following an inflammatory insult. Similar results were obtained with a small molecule inhibitor. Finally, genetic ablation of HuR diminished the amount of RNA decay factors near the NGF receptor, TrkA (Wiesmann et al., 1999). This observation suggests that HuR may ensure that localized populations of mRNA are maintained at appropriate levels required for long-lived changes in nociceptor activity. Collectively, this work reveals a role for HuR in the persistence of pain-associated behavior triggered by inflammatory cues.

Materials and Methods

Experimental animals. All experimental procedures and animal care were authorized by the Institutional Animal Care and Use Committee at the University of Texas at Dallas and the University of Wisconsin–Madison and were conducted according to the guidelines of the

International Association for the Study of Pain. Swiss Webster (catalog #Tac:SW, Taconic Biosciences) and C57BL/6 (catalog #C57BL/6NTac, Taconic Biosciences) mice of both sexes were used. The HuR floxed mice were obtained from The Jackson Laboratory (catalog #021431; Ghosh et al., 2009). The Pirt cre mice were previously described (Kim et al., 2008). Animals were provided with food and water *ad libitum* and were housed in a humidity- and temperature-regulated vivarium.

Molecular cloning. The complete open reading frame of mouse HuR (NP_034615.2) was amplified from cDNA using Phusion DNA Polymerase (catalog #F-530XL, Thermo Fisher Scientific) using the following PCR cycling conditions: an initial denaturation step (98°C for 360 s), subsequent denaturation steps (98°C for 30 s), annealing (55°C for 30 s), extension (72°C for 30 s), and a final extension step (72°C for 240 s). The core iterative cycle was repeated for 30 cycles. The resulting fragment was subcloned into the pGEX-4T vector (catalog #GE28-9545-49, Millipore Sigma) at the XhoI site (catalog #R0146S, New England BioLabs) using Gibson assembly (Gibson et al., 2009). The following primers were used for amplification and recombination with pGEX-4T: 5'-GGATCTGGTTCGCGTGATCCCCGAATTCCCGGGTCGACTCATGTCTAATGGTTATGAAGACCACATG and 5'-GTCAGTCACGATGCGGCCGCTCATGATGATGATGATGCTCTTTGTGGGACTTGTGGTTTTGAA. The ligation was conducted at 50°C degrees for 1 h. The ligated products were then transformed into cold-competent DH5 α cells. Individual colonies were isolated based on ampicillin resistance and subject to validation using Sanger sequencing (Eurofins Genomics).

Protein purification. The BL21 codon plus strain of *Escherichia coli* was transformed with pGEX-4T-HuR and grown on solid media supplemented with ampicillin and chloramphenicol at 37°C for 12 h. Individual colonies were used to inoculate 5 ml starter cultures, which were grown to saturation at 37°C for 14–16 h in media supplemented with ampicillin and chloramphenicol. A 1.0 ml aliquot of the Lysogeny Broth (LB) starter was used to inoculate 1.0 L of LB media supplemented with ampicillin and chloramphenicol. The large-scale cultures were initially grown at 37°C with shaking at 225 rpm for 4.5 h to an optical density of 0.5 at 600 nm. The cultures were then incubated at 15°C for 1 h before induction of protein expression with the addition of IPTG (isopropylthio- β -galactoside) to a final concentration of 0.5 mM (catalog #12481C, GoldBio). Expression was continued for 16 h at 15°C with shaking at 200 rpm. Cells were harvested by centrifugation at 7500 \times g for 30 min. The bacterial pellets were resuspended in 35 ml of resuspension buffer containing 50 mM Tris-HCl, pH 8.0 (catalog # MFCD00004679, Research Products International), 500 mM NaCl (catalog #S23025-500.0, Research Products International), 5 mM dithiothreitol (DTT; catalog #DTT10, GoldBio), 0.2% NP-40 (catalog #85124, Thermo Fisher Scientific), 5% glycerol (catalog 15514011, Thermo Fisher Scientific), 1.0 mM EDTA (catalog #327211000, Thermo Fisher Scientific), 20 mM β -mercaptoethanol (catalog #125470100, Thermo Fisher Scientific), 1.0 mg/ml lysozyme (catalog #L-040-1, GoldBio), 1.0 mM phenylmethylsulfonyl fluoride (PMSF; catalog #P-470-10, GoldBio), and Pierce Protease Inhibitor (catalog #A32963, Thermo Fisher Scientific). The resuspended pellets were sonicated on ice with the following settings: amplitude 70%, pulse on/off cycle for 3 s each for a total time of 2 min. The lysate was then centrifuged at 28000 \times g for 20 min at 4°C to obtain a clear supernatant. This was then layered on top of 2.0 ml of pre-equilibrated glutathione S-transferase (GST) agarose resin (catalog #G-250-5, GoldBio) in a polypropylene chromatography column (catalog #7311550, Bio-Rad). The supernatant was allowed to flow through the resin by gravity at 4°C. The columns were then washed with 100 ml of wash buffer (50 mM Tris-HCl, pH 8.0 (catalog #MFCD00004679, Research Products International), 1 M NaCl (catalog #S23025-500.0, Research Products International), 5 mM DTT (catalog #DTT10, GoldBio), and 5% glycerol (catalog #15514011, Thermo Fisher Scientific)). Proteins were eluted in 4.0 ml of buffer containing reduced glutathione (50 mM Tris-HCl, pH 8.0; catalog # MFCD00004679, Research Products International), 300 mM NaCl (catalog #S23025-500.0, Research Products International), 5 mM DTT (catalog #DTT10, GoldBio), 30 mM reduced glutathione (catalog #G-155-25, GoldBio), and 5% glycerol (catalog #15514011, Thermo Fisher Scientific). Dialysis of the eluted protein was done using snakeskin tubing (catalog #88245, Thermo Fisher Scientific) in 2 L of dialysis buffer (20 mM

Tris-HCl, pH 8.0 (catalog # MFCD00004679, Research Products International), 300 mM NaCl (catalog #S23025-500.0, Research Products International), 0.1 mM PMSF (catalog #P-470-10, GoldBio), and 5% glycerol (catalog #15514011, Thermo Fisher Scientific). Purified protein was concentrated to ~10 mg/ml using concentrator columns (catalog #UFC901024, Millipore Sigma).

In vitro selection and high-throughput sequencing and sequence specificity landscapes. *In vitro* selection and high-throughput sequencing and sequence specificity landscapes (SEQRS) was conducted using purified mouse HuR protein as described (Campbell et al., 2012; Lou et al., 2017). Briefly, an initial RNA library was generated using AmpliScribe T7-Flash Transcription Kit (catalog #NC1559453, Fisher Scientific) from 1.0 µg of double-stranded DNA. Turbo DNase (catalog #AM2238, Thermo Fisher Scientific) was used to remove the DNA template from the RNA library. Two hundred nanograms of RNA was added to HuR (~100 nmole), immobilized onto magnetic GST resin (catalog #78601, Thermo Fisher Scientific). Binding reactions were conducted in 100 µl of SEQRS buffer containing 50 mM HEPES, pH 7.4 (catalog #H4034-100G, Millipore Sigma), 2 mM EDTA (catalog #327211000, Thermo Fisher Scientific), 150 mM NaCl (catalog #S23025-500.0, Research Products International), 0.1% NP40 (catalog #85124, Thermo Fisher Scientific), 1.0 mM DTT (catalog # DTT10, GoldBio), 200 ng tRNA competitor (catalog #AM7119, Thermo Fisher Scientific), and 0.1 U RNase inhibitor (catalog #N2611, Promega). The combined samples were incubated for 30 min at 22°C before magnetic isolation of protein–RNA complexes. The resin was subjected to four washes of 200 µl SEQRS buffer. After the final wash step, the beads were incubated in elution buffer (1.0 mM Tris, pH 8.0; catalog # MFCD00004679, Research Products International) containing 10 pmol of the reverse transcription primer. Samples were heated to 65°C for 10 min and then cooled on ice. The ImProm-II Reverse Transcription kit (catalog #A3800, Promega) was used to obtain single-stranded DNA (ssDNA). The ssDNA was amplified using GoTaq 2X Master Mix kit (catalog #M7123, Promega). After sequencing, logos were generated using the MEME suite (Bailey et al., 2015). To calculate the area under the curve, two likelihood distributions were used. Data were partitioned into test and training sets. The training sets were used to learn the data likelihood function. Using the learned likelihoods and the test dataset, the receiver operating characteristic (ROC) curve was formed for each fold. Finally, the ROCs were averaged over the 10 folds. The total area under the curve was calculated based on a trapezoidal approximation. Frequency distributions of SEQRS sequences in cross-linking immunoprecipitation (CLIP) data were determined based on histograms of cumulative distributions surrounding sites of productive cross-linking across the genome as described (Campbell et al., 2014). The CLIP was obtained from a previous work (Lebedeva et al., 2011).

Primary DRG culture. Swiss Webster mice (4–6 weeks old) were anaesthetized using isoflurane and euthanized via decapitation. DRG were collected aseptically and placed in ice-cold HBSS (catalog #14170112, Thermo Fisher Scientific). The collected tissue was enzymatically dissociated with collagenase A (1.0 mg/ml; catalog #10103578001, Millipore Sigma) for 25 min at 37°C followed by collagenase D (1.0 mg/ml; catalog #11088858001, Millipore Sigma) with papain (30 U/ml; catalog #10108014001, Millipore Sigma) for 20 min at 37°C. DRGs were then triturated in a 1:1 mixture of 1.0 mg/ml trypsin inhibitor (catalog #10109878001, Millipore Sigma) and bovine serum albumin, then filtered through a 70 µm cell strainer (catalog #431751, Corning). Cells were pelleted and resuspended in DMEM/F12 with GlutaMAX (catalog #10565018, Thermo Fisher Scientific) containing 10% fetal bovine serum (catalog #26140079, Thermo Fisher Scientific) and 1.0% penicillin and streptomycin (catalog #15140122, Thermo Fisher Scientific). A combination of 3 µg/ml 5-fluorouridine (catalog #F5130-100MG, Millipore Sigma) and 7 µg/ml uridine (catalog #U3750-100G, Millipore Sigma) was added to the growth media to prevent proliferation of non-neuronal cells. The resuspended cells were evenly distributed onto culture plates coated with poly-D-lysine (PDL; catalog #P6407-5MG, Millipore Sigma) and incubated at 37°C in a humidified 95% air/5% CO₂ incubator.

Human-induced pluripotent stem cell cultures and treatments. The culture conditions for human-induced pluripotent stem cell (hiPSC) sensory neurons and astrocytes were previously described (Chase et al.,

2022). In brief, hiPSC astrocytes (catalog #BX-0600, BrainXell) were subcultured in PDL-treated T75 flasks (catalog #156499, Thermo Fisher Scientific) for 10 d to allow for maturation. They were maintained in DMEM/F-12 (Thermo Fisher Scientific, catalog #11330032), GlutaMAX (catalog #35050061), neurobasal medium (catalog #21103049, Thermo Fisher Scientific), N2 supplement catalog #17502048, Thermo Fisher Scientific), fetal bovine serum (catalog #26140079, Thermo Fisher Scientific), and astrocyte supplement (catalog #BX-0600, BrainXell). hiPSC sensory neuron progenitors (catalog #ax0555-kit, Axol Bioscience) were cocultured simultaneously with matured astrocytes on 0.1% polyethyleneimine (PEI; catalog #408727-100ml, Sigma-Aldrich) and 25 µg/ml laminin (catalog #L4544-100ul, Sigma-Aldrich) pretreated 48-well multielectrode array (MEA) plates (catalog #M768-tMEA-48W, Axion Biosystems) according to the Axol seeding protocol. Cultures were subjected to 50% medium exchange every other day for 43 d using Axol Neuronal Maintenance Medium supplemented (catalog #ax0031a, Axol Bioscience) with NGF, NT-3, BDNF, GDNF, 1× penicillin-streptomycin (catalog #15140122, Thermo Fisher Scientific), and ROCK inhibitor (Y27632; catalog #Y0503-1mg, Sigma-Aldrich).

Multielectrode arrays. MEA experiments were performed as described previously with minor modifications (Barragan-Iglesias et al., 2021). MEA plates (48 wells; catalog #M768-tMEA-48W, Axion Biosystems) coated with 0.1% PEI (catalog #408727-100ml, Sigma-Aldrich) and 20 µg/ml laminin (catalog #L4544-100ul, Sigma-Aldrich) were used to support the growth of DRG neurons. Neuronal cells were seeded onto these plates at 40,000 neurons per well in growth medium supplemented with 5 ng/ml GDNF (catalog #NBP2-61336-10ug, Novus Biologicals). Cultures were grown at 37°C, 5% CO₂, and 95% humidity. Spontaneous extracellular recordings were conducted using an Axion Maestro recording system (Axion Biosystems). Continuous recordings were simultaneously collected from all 48 wells at a 12.5 kHz sampling rate. Extracellular spikes were classified as filtered continuous data that exceeded an adaptive threshold of $\pm 5.5 \sigma$ based on 1 s snapshots of root mean square (rms) noise. Active electrodes were defined as those that recorded a minimum of one spike per minute during baseline spontaneous extracellular recordings. Spontaneous neuronal activity was recorded on alternate days. On the fifth day, neuronal activity was recorded to confirm viability and obtain a stable spontaneous baseline. MEA recordings were conducted on cultures with at least one spontaneously active electrode per well between day *in vitro* 9 and 15. Cultures were maintained at 37°C, 5% CO₂, and 95% humidity throughout the recording. Before the inclusion of any drugs, a 30 min baseline recording was collected. For subsequent tests, only wells with spontaneously activate electrodes were used. Following drug treatment, samples were allowed to rest for 10 min before collecting 30 min recordings. Mean firing rates of each treatment group were normalized to its baseline firing rate and presented as relative to the vehicle group. For the hiPSC samples, spontaneous baseline recordings were captured every alternate day to determine a stable activity baseline for experiments. This was defined as three consecutive recordings exhibiting no statistically significant change in either active electrode yield or mean firing rate. For each new recording session, MEAs were allowed to acclimate for 30 min with stage-top CO₂ and temperature control. Extracellular action potential (EAP) recordings were conducted for all electrodes and all wells simultaneously at a 12.5 kHz sampling rate. EAPs were detected using an adaptive threshold set to 5.5σ relative to the rms noise band. Threshold crossing time stamps and associated waveforms were captured for further analysis. Mean firing rates were calculated using Axion Neural Metric Tool software and normalized to their respective baselines, acquired immediately before treatment.

Immunocytochemistry. Cultured primary DRG neurons were plated on eight-well chambered slides (catalog #12-565-8, Fisher Scientific). Cultures were rinsed with ice-cold 1× PBS and fixed in ice-cold 4% PFA (catalog #28906, Thermo Fisher Scientific) in 1× PBS for 20 min. The cells were washed three times with 1× PBS under gentle agitation. Cells were permeabilized with 0.3% Triton X-100 (catalog #T8787-250ml, Millipore Sigma) in 1× PBS for 10 min. After three consecutive washes with 1× PBS, slides were blocked with 10% NGS (catalog #005-000-121,

Jackson ImmunoResearch) and 1% BSA (catalog #J10856.22, Thermo Fisher Scientific) in 1× PBS for 1 h at room temperature. Primary antibodies were diluted in blocking solution: peripherin (1:1000; catalog #NBP1-05423, Novus Biologicals), GW182 (1:200; catalog #sc-56314, Santa Cruz Biotechnology), and DCP1 (1:300; catalog #sc-100706, Santa Cruz Biotechnology). Cells were incubated with primary antibodies at 4°C overnight in a humidified chamber. Following three consecutive washes with 1× PBS, appropriate secondary antibodies were diluted in blocking solution (Alexa Fluor, Invitrogen) and were applied for 1 h at room temperature. Following additional 1× PBS washes, coverslips were mounted with ProLong Glass (catalog #P36984, Thermo Fisher Scientific).

Immunohistochemistry. Mice were anesthetized with isoflurane and killed by cervical dislocation. Tissues (dorsal root ganglion, sciatic nerve, and spinal cord) were flash frozen in Tissue-TeK optimal cutting temperature compound (catalog #NC9806257, Fisher Scientific) on dry ice. The tissues were processed into 20 μm sections using a cryostat and mounted onto SuperFrost Plus slides (catalog #22-037-246, Fisher Scientific). Tissue sections were fixed with ice-cold 4% PFA (catalog #28906, Thermo Fisher Scientific) in 1× TBS for 20 min at room temperature. Following three consecutive washes with wash buffer (1× TBS plus 0.025% Triton X-100), sections were permeabilized with 0.3% Triton X-100 (catalog #T8787-250ml, Millipore Sigma) in 1× TBS for 10 min. Samples were then washed three times with wash buffer and blocked for 2 h with Goat Anti-Mouse Fab Fragment (catalog #115-007-003, Jackson ImmunoResearch) in 1× TBS in a humidified chamber at room temperature. Sections were washed twice with wash buffer to remove unbound Fab Fragments. The slides were blocked with 10% NGS and 1% BSA in 1× TBS for 2 h in a humidified chamber at room temperature. Primary antibodies were diluted in 10% NGS (catalog #005-000-121, Jackson ImmunoResearch) and 1% BSA (catalog #J10856.22, Thermo Fisher Scientific) in 1× TBS; ELAVL1 (1:100; catalog #A-21277, Invitrogen), peripherin (1:1000; catalog #NBP1-05423, Novus Biologicals), NF-200 (1:750; catalog #N4142, Sigma-Aldrich), NeuN (1:1000; catalog #266004, Synaptic Systems), CGRP (calcitonin gene related peptide polyclonal; 1:200; catalog #BML-CA1134-0100, Enzo), Isolectin B4 (1:1000; catalog #I21412, Invitrogen), Beta-III-Tubulin (1:1000; catalog #302304, Synaptic Systems), GFAP (1:1000; catalog #pa5-16291, Invitrogen), and IBA1 (1:500; catalog #234009, Synaptic Systems). Slides were incubated with primary antibodies at 4°C overnight in a humidified chamber. The slides were washed three times with wash buffer. Appropriate secondary antibodies (Alexa Fluor, Invitrogen) were diluted in blocking solution and applied for 1 h at room temperature. Following additional 1× TBS washes, coverslips were mounted with ProLong Glass (catalog #P36984, Thermo Fisher Scientific).

Proximity ligation assay (PLA). Cultured primary DRG neurons were plated on eight-well chambered slides (catalog #12-565-8, Fisher Scientific). Proximity ligation assays were conducted using the Duolink Proximity Ligation Assay kit (catalog #DUO92101-1KT, Thermo Fisher Scientific). Cultures were rinsed with ice-cold 1× PBS and fixed in ice-cold 4% PFA (catalog #28906, Thermo Fisher Scientific) in 1× PBS for 20 min. The cells were washed three times with 1× PBS under gentle agitation. Cells were permeabilized with 0.3% Triton X-100 (catalog #T8787-250ml, Millipore Sigma) in 1× PBS for 10 min. After three consecutive washes with 1× PBS, cells were blocked with kit-provided blocking solution for 1 h at 37°C. Primary antibodies were diluted in kit-provided antibody diluent containing the following: ELAVL1 (1:100, catalog #A-21277, Invitrogen), TrkA (1:200; catalog #06-574, Millipore Sigma), GW182 (1:200; catalog #sc-56314, Santa Cruz Biotechnology), DCP1 (1:300; catalog #sc-100706, Santa Cruz Biotechnology) and peripherin (1:1000; catalog #NBP1-05423, Novus Biologicals). The cells were incubated with primary antibodies overnight at 4°C. The subsequent steps for the assay followed the guidelines from the manufacturer. On completion of the assay, cells were stained with DAPI (1:5000) in 1× PBS, and coverslips were mounted on the slides using ProLong Glass (catalog #P36984, Thermo Fisher Scientific).

Image acquisition and data analysis. All images were acquired using an Olympus FV3000 Laser Scanning confocal microscope on a 40×

plus 1.5× (zoom) or 20× objective for imaging cells or tissues, respectively. Z-projections for immunocytochemistry and proximity ligation assay (PLA) images were obtained with FluoView (Olympus) software. Image analysis was done using Fiji. PLA puncta were quantified for individual cells. For quantification purposes, a region of interest was manually drawn surrounding the soma of a peripherin-positive cell. Background signal was subtracted using a rolling ball radius of six. A threshold was applied before the image was converted to a mask. The Analyze Particles tool was then used to count PLA puncta larger than 0.1 μm² with circularity >0.6. Fluorescence intensity was quantified using the corrected total cell fluorescence method. Colocalization was calculated using the plug-in JaCoP, and Pearson's coefficient of correlation was used.

NGF and IL-6 models of hyperalgesic priming. To investigate the role of HuR in pain-associated behavior, we used the mouse model for hyperalgesic priming originally developed by Reichling and Levine (2009). In brief, calibrated von Frey filaments (catalog # 37450-275, Ugo Basile) were used to measure the mechanical hypersensitivity of mice. Mice were habituated in acrylic boxes with wire mesh floors for 30 min. Von Frey filaments were applied on the hindpaw of mice for 3 s, and using the up-down method, withdrawal thresholds were calculated (Chaplan et al., 1994). Animals were injected with either NGF (50 ng) or IL-6 (1.25 ng) in 25 μl saline into the right hindpaw. Measurements were made at various time points post-NGF and IL-6 administration. On day nine, priming was evoked with a subthreshold dose of PGE-2 (100 ng) by intraplantar (i.pl.) injection into the ipsilateral hind paw (Kandasamy and Price, 2015). All assignments of treatments and the measurements were fully randomized. All behavioral observations were made by experienced experimenters who were blinded to the experimental conditions.

Data and statistical analysis. The data and statistical analysis comply with the recommendations on experimental design and analysis in pharmacology (Curtis et al., 2018). Data are presented as mean ± SEM of at least six animals per group. The sample size was estimated as $n = 6$ using G*power (RRID:SCR_013726) for a power calculation with 80% power, expectations of 50% effect size, with α set to 0.05. Exact numbers of samples per group are shown in the figure legends. GraphPad Prism version 9.0 (GraphPad Software, RRID:SCR_002798) was used for graph plotting and statistical analysis. The Student's *t* test was used to compare two independent groups. Statistical evaluation for three or more separate groups was performed by one-way or two-way ANOVA, followed by Sidak's multiple-comparisons test, and the a priori level of significance at 95% confidence level was considered at $p < 0.05$. Appropriate diagnostic statistics were conducted to ensure valid use of parametric statistics.

Results

Preferentially translated transcripts harbor U-rich elements

Previously, we examined translation of mRNAs after a brief treatment containing NGF and IL-6 (de la Peña et al., 2021a). Among the transcripts with increased translation, we performed motif discovery in the 3'UTR using the MEME suite (Bailey et al., 2015). We found that a U-rich element was significantly enriched (Extended Data Fig. 1-1). The next challenge was to identify factors that might decode this information in sensory neurons. We elected to focus on HuR as a potential trans-acting factor for three reasons. First, HuR has been implicated in the stabilization and translational enhancement of targeted mRNAs (Peng et al., 1998; Mazan-Mamczarz et al., 2003; Kumar et al., 2021). Second, it generally binds to U-rich sequences situated in the 3'UTR (Lebedeva et al., 2011; Mukherjee et al., 2011; Nadar et al., 2011; Matoukova et al., 2012). Third and finally, HuR has been implicated in certain forms of plasticity in the CNS (He et al., 2019).

To define the specificity of HuR in an unbiased manner, we capitalized on an *in vitro* selection and high-throughput

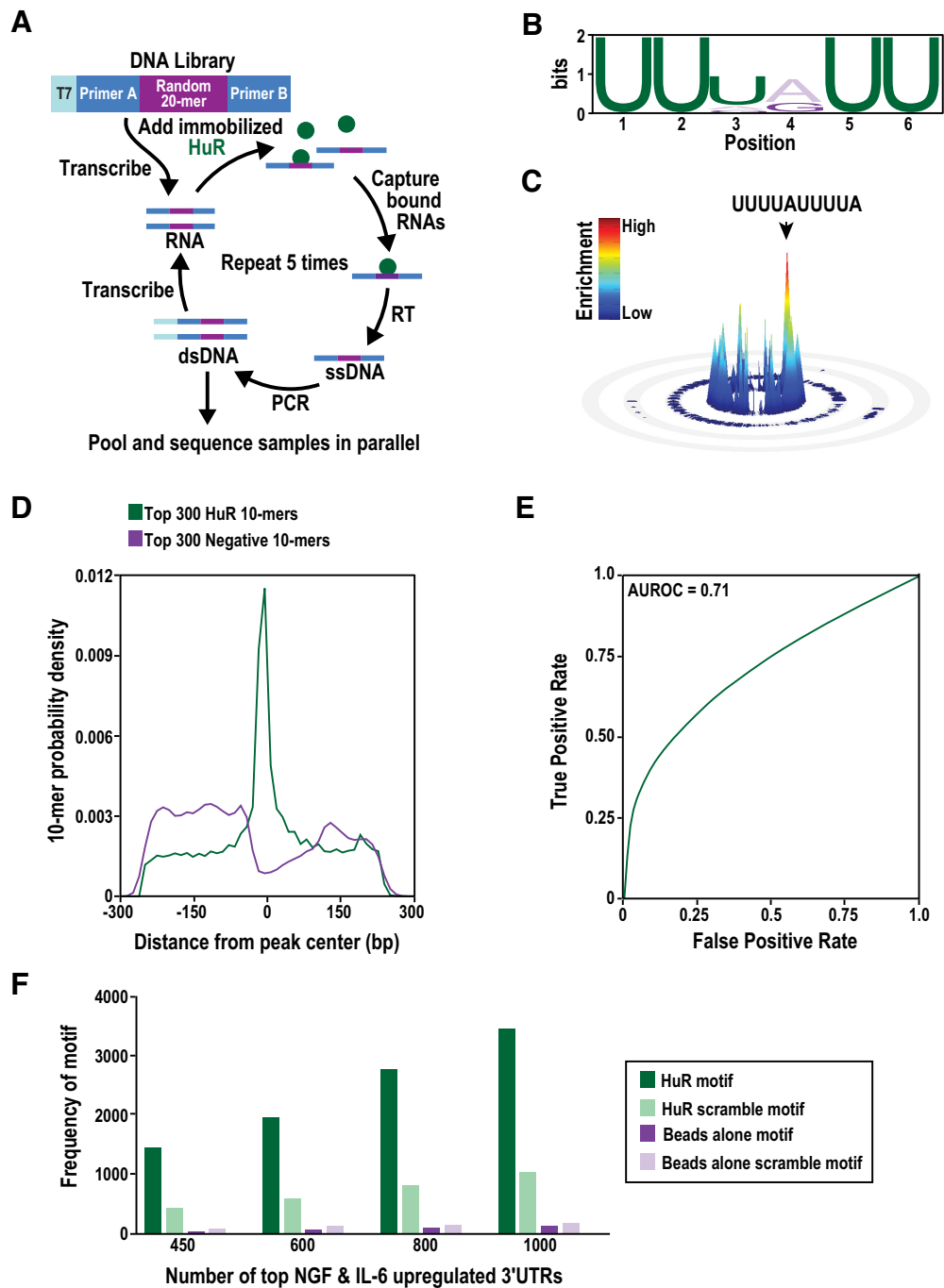


Figure 1. An AU-rich element (ARE) recognized by HuR is enriched in the 3'UTR of transcripts preferentially translated by NGF and IL-6. **A**, A schematic of the SEQRS strategy. An RNA library is generated from T7 transcription of a randomized DNA 20-mer (purple). The library is incubated with HuR immobilized to magnetic resin (solid green circles). RNA-protein complexes are isolated following consecutive wash steps, and bound RNAs are eluted. The eluted RNA is reverse transcribed, and the T7 promoter is reintroduced through PCR. This process is repeated for five rounds before Illumina-based high-throughput sequencing. **B**, A sequence logo generated from MEME (Bailey et al., 2015) using reads obtained through SEQRS. **C**, A sequence specificity landscape plot for an enriched AU-rich motif obtained from SEQRS. All the data in the experiment were fit to the consensus element UUUUAUUUUA. The inner ring represents perfect matches to that element in the observed data with concentric rings outward representing one mismatch per ring. The lack of data in outer rings suggests that the consensus motif is highly enriched. **D**, Enrichment of the 300 most enriched 10-mer sequences for either HuR (green) or a set of random sequences (purple) in HuR CLIP binding sites (Lebedeva et al., 2011). The statistical comparison was made using the Wilcoxon–Mann–Whitney rank sum test. **E**, Receiver operating characteristic curve analyses of the HuR motif. **F**, Enrichment of motifs in mRNAs with increased translation in response to inflammatory cues (de la Peña et al., 2021a). A motif containing poly(U) obtained from the prior ribosome profiling dataset is provided in Extended Data Figure 1-1. HuR (dark green) compared with a scramble motif (light green). Halo tag motif is a motif-obtained protein tag only (control sample) from SEQRS. A motif obtained from mRNAs with increased translation.

sequencing method called SEQRS (Fig. 1A). This approach has been used to examine individual proteins, protein complexes, and structured RNA elements and in defining the effects of mutations on specificity (Campbell et al., 2012;

LeGendre et al., 2013; Campbell et al., 2014; Weidmann et al., 2016; Lou et al., 2017; Barragán-Iglesias et al., 2018; Zhou et al., 2018; Qiu et al., 2019; Wolfe et al., 2020). In brief, recombinant HuR was immobilized on beads and incubated

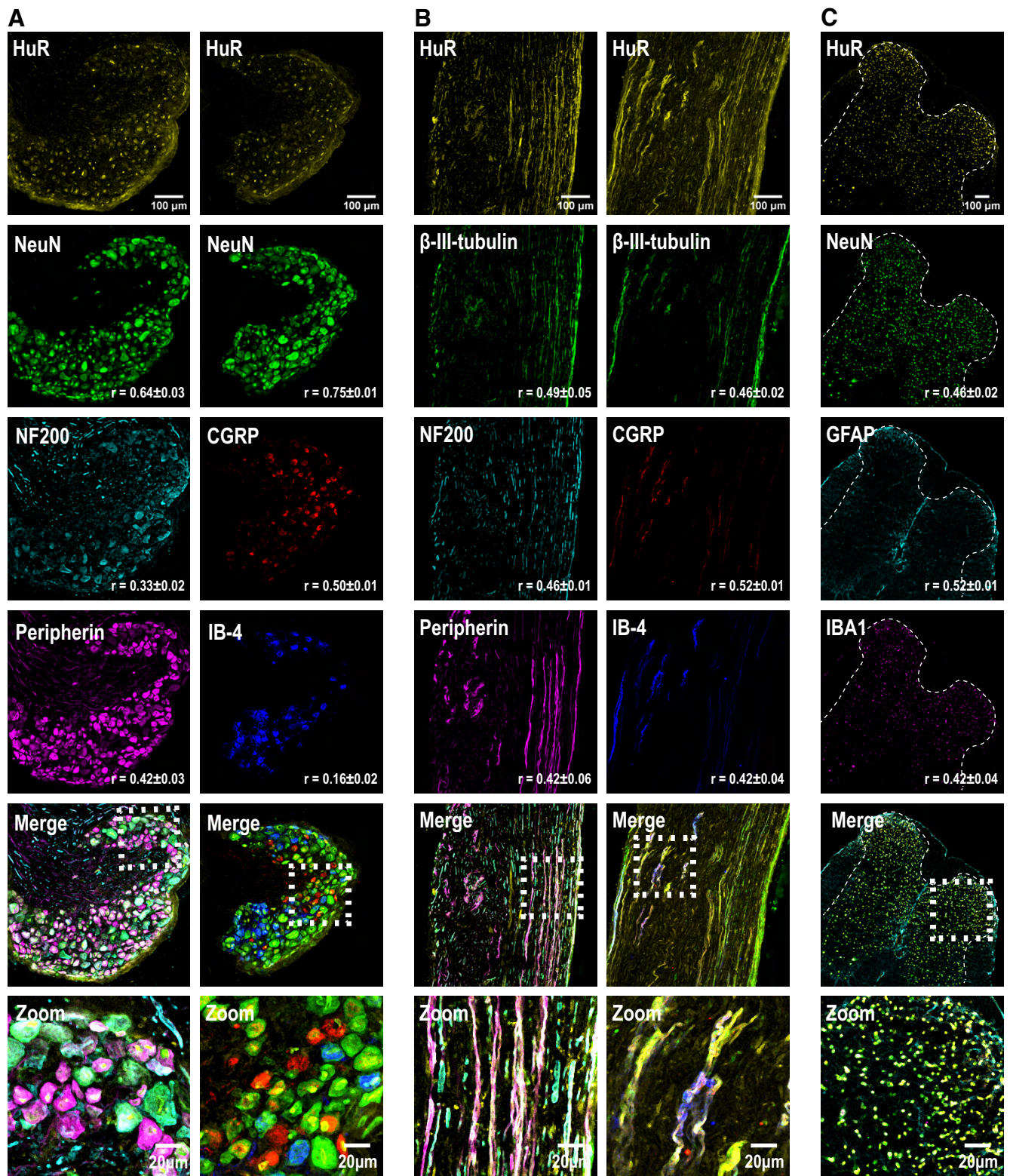


Figure 2. HuR is expressed in most populations of sensory neurons. **A**, HuR (yellow) is highly expressed in sensory neurons found in the DRG and colocalizes with NeuN (green), a pan-neuronal marker. It also colocalizes with other neuronal markers that include NF-200 (a marker of large, myelinated neurons, cyan), CGRP (a marker of peptidergic neurons, red), peripherin (a marker of unmyelinated neurons, magenta), and IB4 (a marker of nonpeptidergic neurons, blue). **B**, HuR (yellow) is highly expressed in the sciatic nerve and colocalizes with β -III-tubulin (green), a pan-neuronal marker. **C**, HuR (yellow) is also expressed in various cell populations found in the dorsal horn of the spinal cord. It colocalizes with NeuN (a pan-neuronal marker, green), GFAP (a marker of astrocytes, cyan), and IBA1 (a marker for macrophages and microglia, magenta). The Pearson's correlation coefficients are reported in the bottom right corner (**A**, **B**). Scale bars: 100 μ m for full size image and 20 μ m for zoomed image.

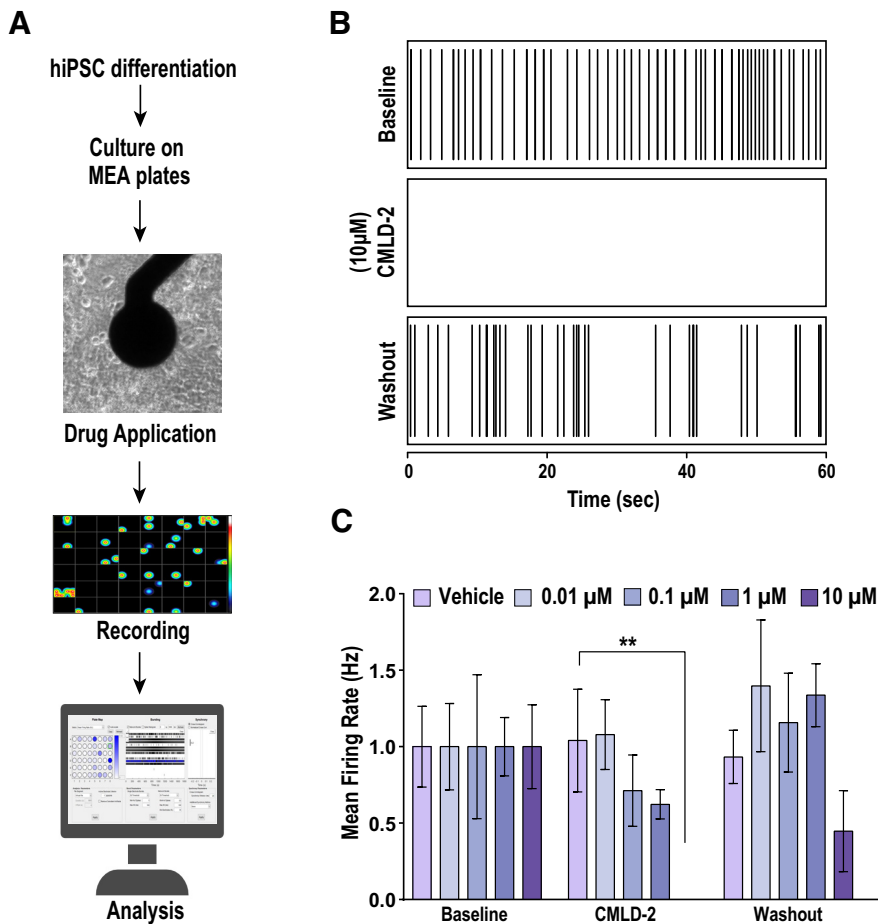


Figure 3. CMLD-2 causes a reduction in neuronal firing in hiPSC-derived sensory neurons. **A**, A schematic representation of the MEA experiment. Sensory neurons derived from hiPSCs are cultured on plates embedded with electrodes. Basal mean firing rates were assessed, followed by treatments. Data were processed using the Axion Maestro software. **B**, Raster plots for representative single-electrode recordings of neuronal firing for baseline, CMLD-2 treated, and postwashout of CMLD-2 over a 1 min period in hiPSC-derived sensory neurons. The drug was washed out with a complete media exchange. **C**, Drug treatments consisted of either CMLD-2 (0.01, 0.1, 1, or 10 μM) or vehicle (0.1% DMSO). CMLD-2 inhibits baseline neuronal firing rates in hiPSC-derived sensory neurons in a dose-dependent manner. CMLD-2 at 10 μM silenced firing, which was restored on drug washout. Data represented are individual values with mean \pm SEM; $n = 4$; $**p < 0.01$, one-way ANOVA followed by Tukey's *post hoc* test. Data obtained from murine DRG sensory neurons is provided in Extended Data Figure 3-1.

with a library containing a 20-nucleotide random region. After incubation, unbound mRNAs were removed through buffer exchange. The enriched pool was then reverse transcribed and amplified so that the T7 promoter sequence was reintroduced. The library was then transcribed again, and the selection process was repeated for five rounds. Sequencing was conducted using the Nextseq 500 Illumina platform. The consensus binding element for HuR was generated from the top 300 most enriched 10-mer sequences using MEME (Fig. 1B; Bailey et al., 1995). It contains a U-rich element with modest enrichment of a purine at position +4 in the five-base motif. This is reminiscent of motifs reported previously (Ray et al., 2009; Lebedeva et al., 2011). To visualize the enrichment of the consensus binding element to all the 10-mers observed in our experiment, we generated a specificity landscape (Fig. 1C). In this plot, all sequence permutations that contain the HuR consensus (UUURUU) are plotted in the inner ring. The outer rings contain increasing numbers of mismatches to the innermost seed sequence; that is, sequences with up to three mismatches are depicted. The z-axis indicated the number of reads for a given sequence normalized to the initial library. The distribution of the data indicates that the consensus

element for HuR is strongly enriched with a relatively low signal for sequence variants with more than a single mismatch. We next asked whether the SEQRS data are enriched in HuR binding sites *in vivo* (Lebedeva et al., 2011). The motif obtained from SEQRS correctly identified the sites obtained from CLIP (Wilcoxon–Mann–Whitney rank sum test $p < 0.01$; Fig. 1D). To address whether the SEQRS motif was a useful predictive tool, we calculated receiver operating characteristic curves for where an area under the curve of 0.5 suggests no discrimination, 0.7–0.8 indicates acceptable prediction, and any value above 0.8 is excellent. The value we observed (0.71) was suggestive of predictive value (Fig. 1E). Finally, we asked whether the HuR motif is enriched in mRNAs whose translation is increased in response to NGF and IL-6 (de la Peña et al., 2021a). A search was conducted for the HuR consensus or a mutant where the U bases are switched to A bases. As additional specificity controls, a background motif found after sequencing RNAs found on empty resin or a permutation of that motif were used as search models. Both the HuR motif and the U to A version of that motif were enriched in transcripts with increased translation following treatments with NGF and IL-6 (Fig. 1F). This indicates that the 3'UTRs are A/U rich, consistent with their known composition. Additionally, the HuR motif was highly enriched, which is suggestive of a biochemical potential for regulatory interactions.

HuR is expressed in most populations of sensory neurons in the DRG

We sought to characterize the distribution of HuR throughout the Peripheral Nervous System (PNS). We examined the DRG, sciatic nerve, and spinal cord using immunohistochemistry (Fig. 2). HuR is present in DRG neurons that immunoreact with NeuN (Fig. 2A). HuR also colocalized with peripherin, a marker for small and medium diameter unmyelinated sensory neurons that are mostly nociceptors (Crawford and Caterina, 2020; Deshmukh et al., 2016). HuR is also expressed in CGRP-positive nociceptors, which are medium-diameter thinly myelinated A δ fibers. HuR colocalized with NF200, a marker of large diameter neurons with myelinated A β fibers and involved in proprioception (Perry et al., 1991; Ishikawa et al., 2005; Crawford and Caterina, 2020). HuR weakly colocalized with IB4, a marker of nonpeptidergic neurons (Silverman and Kruger, 1990; Stucky and Lewin, 1999; Crawford and Caterina, 2020). In the sciatic nerve (Fig. 2B), HuR colocalized with IB4 and CGRP. We included an additional neuronal marker, β -III Tubulin, which is useful for identification of afferent fibers. It was also colocalized with HuR. This is notable as the existence of HuR within the sciatic nerve fibers suggests that it might be involved in mRNA control at local sites of protein synthesis. In the spinal cord, HuR is expressed in neurons that immunoreact with a NeuN antibody, (Fig. 2C) as

well as astrocytes that express GFAP and microglia that express IBA1 (Ahmed et al., 2007). The data indicate that HuR is broadly expressed and is present in the soma and fibers of nociceptive sensory neurons.

Pharmacological inhibition of HuR leads to silencing of neuronal firing

To determine what role, if any, HuR plays in nociceptor function, we capitalized on an inhibitor of HuR, CMLD-2, that prevents its physical association with RNA (Wu et al., 2015). We used this tool to ask whether inhibition of HuR modulates nociceptor activity. To measure action potentials, we cultured neurons on MEAs. These devices consist of a culture dish that contains embedded microelectrodes that monitor extracellular firing events. MEAs have been used to examine excitability of DRG neurons derived from murine and hiPSC models (Fig. 3A; Black et al., 2018, 2019; Chase et al., 2022). We made use of an hiPSC model containing a mixture of sensory neurons and spinal astrocytes (Chase et al., 2022). The inclusion of the latter improves the stability, activity, and differentiation of the sensory neurons. Spontaneous firing in human sensory neurons correlates with pain in humans (Kleggetveit et al., 2012; North et al., 2022). The modest spontaneous activity observed in the hiPSC model was reduced by CMLD-2 in a dose-dependent manner (Fig. 3B,C). Interestingly, CMLD-2 at a concentration of 10 μ M leads to a dramatic reduction in firing. We found that this was reversible, as activity did not significantly differ from the vehicle-treated group following washout of the CMLD-2. We repeated these experiments in primary cultures obtained from murine DRGs and observed qualitatively similar results (Extended Data Fig. 3-1A,B). Collectively, these data indicate that the responsiveness of sensory neurons to HuR inhibition is similar between mice and human models.

Disruption of HuR reduces mechanical hypersensitivity in mice

A standard approach for assessment of allodynia in mice and humans involves quantification of mechanical withdrawal thresholds after application of a von Frey filament. In our assays, filaments of various thickness are applied to the hindpaw until paw flinching is observed. A sufficient amount of force is applied to induce bending of the filament. Based on the gauge of the filament, the amount of force required to elicit a behavioral response can be quantified. Under baseline conditions (no stimuli), ~1.0–1.5 g of pressure is required to trigger a withdrawal. Noxious cues can result in heightened sensitivity. When paired to either pharmacologic or genetic perturbations, changes in withdrawal threshold can be interpreted as either analgesic

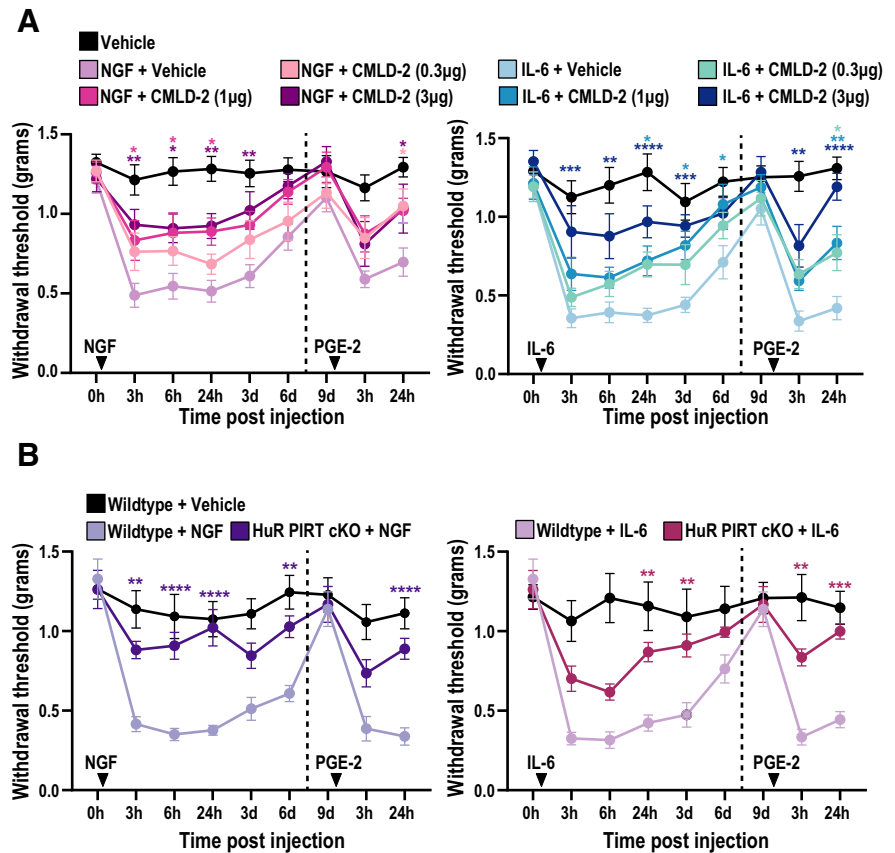


Figure 4. Inhibition or conditional knockout of HuR alleviates NGF or IL-6 induced mechanical hypersensitivity. NGF or IL-6 was injected into the hindpaw of mice. Mice were habituated, and withdrawal threshold was determined using calibrated von Frey filaments at various time points postinjection. After recovery of baseline threshold, a subthreshold dose of PGE-2, i.p., was injected into the hindpaw of mice. Withdrawal threshold was again measured for various time points postinjection. **A**, CMLD-2 attenuated NGF (left), and IL-6 (right) induced mechanical hypersensitivity during the acute and priming phase in male mice. CMLD-2 was coinjected with NGF or IL-6. Data are presented as means \pm SEM; $n = 10$ animals per group; $*p < 0.05$, $***p < 0.01$, $****p < 0.001$, $*****p < 0.0001$, two-way ANOVA with Sidak's multiple-comparisons test (NGF data, vehicle vs CMLD-2, $F_{(8,404)} = 14.77$, $p < 0.0001$; IL-6 data, vehicle vs CMLD-2, $F_{(8,405)} = 22.27$, $p < 0.0001$). **B**, Genetic ablation of HuR from sensory neurons attenuated NGF (left), and IL-6 (right) induced mechanical hypersensitivity during the acute and priming phase in male mice. Data are presented as means \pm SEM; $n = 6/8$ animals per group; $*p < 0.05$, $**p < 0.01$, $***p < 0.001$, $****p < 0.0001$, two-way ANOVA with Sidak's multiple-comparisons test (NGF data, wild-type vs HuR cKO, $F_{(2,163)} = 89.93$, $p < 0.0001$; IL-6 data, wild-type vs HuR cKO, $F_{(2,163)} = 79.39$, $p < 0.0001$). Data are provided for female mice in Extended Data Figure 4-1. Validation of the HuR conditional knockout is provided in Figure 4-2.

(increased withdrawal threshold) or allodynic (decreased withdrawal threshold). Intraplantar injections to the hindpaw with inflammatory mediators (NGF and IL-6) lead to a reduction in withdrawal threshold and increased mechanical hypersensitivity. After resolution of the initial stimuli, a subthreshold injection of PGE-2 (100 ng) results in prolonged hypersensitivity. A similar treatment has only a transient effect in naive mice. This is referred to as hyperalgesic priming and is used as a model of the transition from acute pain to chronic pain (Ferrari et al., 2015; Kandasamy and Price, 2015).

To determine whether transient inhibition of HuR diminishes priming, CMLD-2 was injected with either NGF or IL-6. In both cases, we found that mechanical hypersensitivity was decreased in a dose-dependent manner in male mice with a peak effect at 3 μ g (Fig. 4A). We repeated these experiments in female mice at the 3 μ g dose and observed a similar outcome with both stimuli (Extended Data Fig. 4-1A). In both sexes, we found that CMLD-2 caused significant reduction in mechanical hypersensitivity in both the acute and primed phase. This suggests that an HuR inhibitor diminishes nociceptive responses to inflammatory mediators and is not sexually dimorphic.

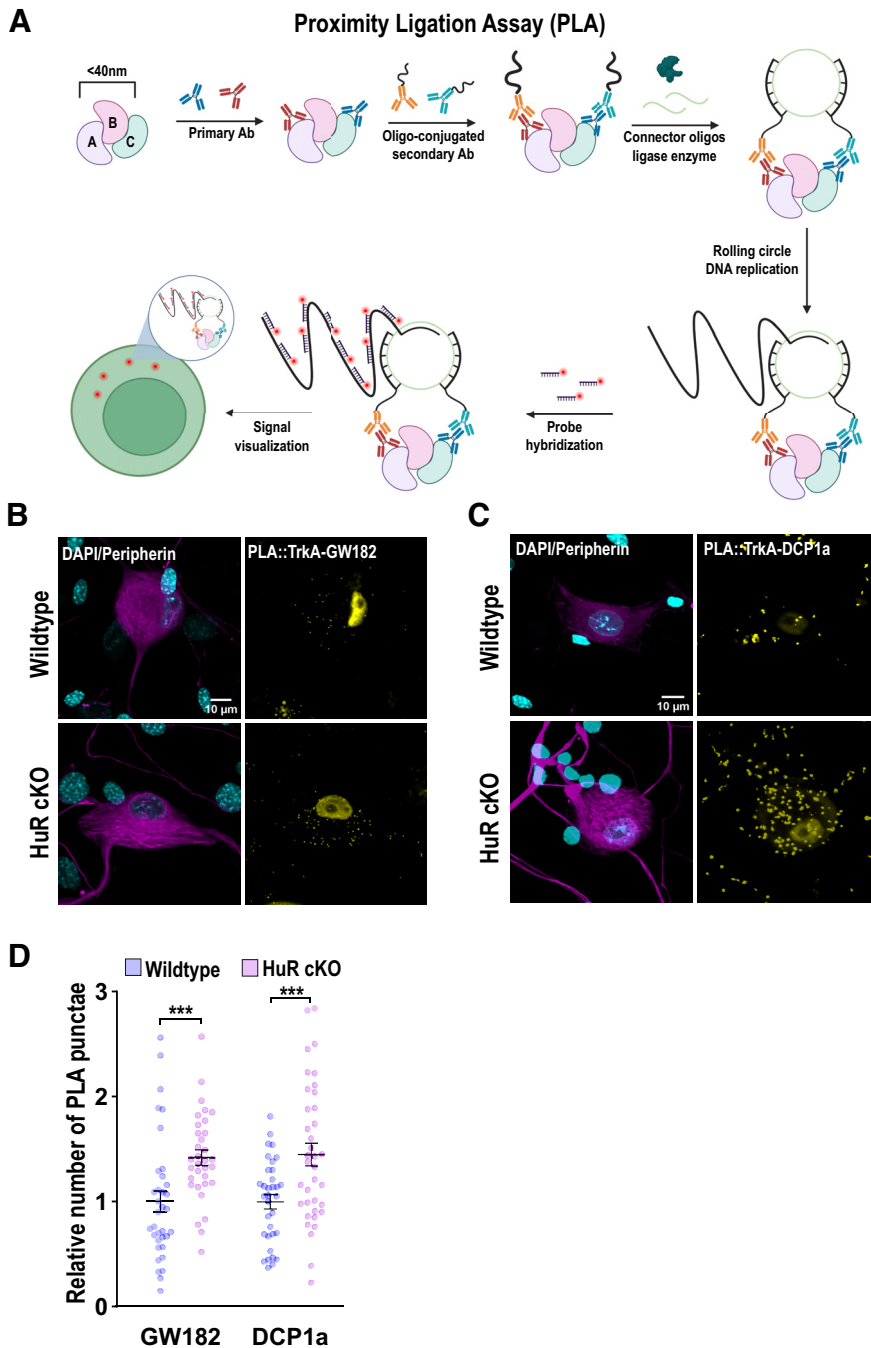


Figure 5. Association of HuR with the TrkA receptor in cultured mouse DRG neurons decreases TrkA interactions with DCP1a and GW182. **A**, A schematic of the PLA approach to quantify the spatial coupling of proteins (<math><40\text{ nm}</math>). Primary antibodies are used to localize proteins of interest. Oligo-conjugated secondary antibodies bind their primary targets. Ligation is used to generate a replication template for rolling circle replication. Dye-conjugated DNA probes hybridize the amplified products and enables quantification of protein–protein proximity. **B**, Genetic loss of HuR increases TrkA–GW182 association in peripherin-positive neurons. Peripherin is stained in magenta and DNA stained with DAPI is shown in blue. Yellow indicates the PLA signal. Scale bars: 10 μm . **C**, Genetic loss of HuR increases TrkA–DCP1a association in peripherin-positive neurons. **D**, Quantification of PLA puncta per square micrometer among TrkA–Ago2, GW182, or DCP1a in wild-type and HuR cKO cultured mouse DRG neurons. Each data point is the total number of PLA puncta within one cell. Data are presented as means \pm SEM; $n = 34\text{--}37$ cells per group; *** $p < 0.01$ **** $p < 0.001$, two-tailed Student's t test with Welch's correction (GW182 data, wild type vs HuR cKO, $t = 3.390$, $df = 61.48$; DCP1a data, wild type vs HuR cKO, $t = 3.518$, $df = 60.04$). Quantification of the HuR–TrkA interaction by PLA and total levels for GW182 and DCP1a are provided in Extended Data Figure 5-1.

We next asked whether neuronal HuR is important for behavioral responses to noxious stimuli. To address this question, we generated a mutant animal where a floxed HuR is deleted from sensory neurons using expression of Cre recombinase

driven by the DRG neuron-specific *Pirt* promoter (Kim et al., 2008; Ghosh et al., 2009). We refer to the resulting strain as the HuR conditional knockout (cKO). To validate the HuR cKO, immunohistochemical analyses were conducted on DRG tissues. The amount of HuR reactivity was diminished significantly (Extended Data Fig. 4-2). Next, we examined whether mechanical hypersensitivity was reduced in these animals. Indeed, hyperalgesic priming by NGF and IL-6 was disrupted following removal of HuR from sensory neurons in both male (Fig. 4B) and female (Extended Data Fig. 4-1B) mice. These results suggest that HuR expressed specifically in sensory neurons contributes to mechanical hypersensitivity induced by inflammatory mediators in both sexes.

Loss of HuR alters the proximity of repressive factors and TrkA

To better understand the mechanistic basis for insensitivity of HuR cKO mice to inflammatory mediators, we asked whether factors that repress mRNA stability and translation are abnormally distributed. We reasoned that because HuR antagonizes factors involved in mRNA repression, their accumulation near sites of receptor proximal translation might be altered in the absence of HuR (Kundu et al., 2012). We focused specifically on TrkA because it is the receptor for NGF and colocalizes with HuR (Extended Data Fig. 5-1A). To quantify the interaction between TrkA and RNA-binding proteins, we make use of PLAs (Söderberg et al., 2006; Fig. 5A). In these experiments, interactions between proteins within 40 nm are detected using a pair of antibodies. We examined two factors implicated in mRNA destabilization and translational repression—GW182 and Dcp1a. HuR displaces the miRNA-induced silencing complex (miRISC; Kundu et al., 2012). GW182 is a component of the miRISC. It represses translation and stimulates shortening of the poly(A) tail (Braun et al., 2011; Chekulaeva et al., 2011). An important consequence of deadenylation is decapping (Behm-Ansmant et al., 2006; Chekulaeva et al., 2011). The latter is catalyzed by the Dcp1/Dcp2 complex. We found that the amount of GW182 and Dcp1a near TrkA was significantly increased following genetic loss of HuR (Fig. 5B–D). Importantly, loss of HuR did not change the total abundance of either GW182 or Dcp1a (Extended Data Fig. 5-1B–D). Collectively, these results suggest that HuR antagonizes mRNA repression near TrkA.

Discussion

Four major findings emerged from this work. First, HuR is broadly expressed in the DRG and is present in the soma and axons of nociceptors. Second, inhibition of HuR reduces nociceptor activity in both human and mouse sensory neurons. Third, genetic elimination or transient inhibition of HuR robustly attenuates pain associated behaviors in male and female mice. Fourth and finally, the localization of mRNA repressive factors near TrkA is abnormal following loss of HuR. We discuss the implications of each observation in turn.

Plasticity in nociceptors hinges on precise control of translation. RNA-binding proteins play integral roles in the control of mRNA fate. Nociceptors are an attractive system for probing the role of RNA-binding proteins in activity-dependent mRNA control. Afferent nerve fibers are among the largest in the human body, and long-lived changes in their excitability evoked by noxious cues hinge on *de novo* protein synthesis (Melemedjian et al., 2010; Ferrari et al., 2013; Barragán-Iglesias et al., 2018; Chase et al., 2022). We previously examined translation in DRG neurons treated with inflammatory mediators using ribosome profiling and noted enrichment of a U-rich sequence the 3' UTRs of preferentially translated mRNAs (de la Peña et al., 2021a). In parallel, we identified a consensus binding element for HuR using selection and high-throughput sequencing that is similarly enriched in uridines. This suggested that HuR might play a role in post-transcriptional responses to inflammatory cues. A major caveat to these observations is the fact that multiple RNA-binding proteins recognize a similar element. For instance, there are three members of the Hu family (HuB/Hel-N1, HuD, and HuC) that are present in neurons and bind AU rich elements (Park et al., 2000). HuR has been linked to the production of inflammation mediators in a neuropathic pain model (Sorge et al., 2022). Yet, its roles in peripheral neurons are unclear. A major goal of this work was to ask specifically whether HuR is present in nociceptors and if it is important to their function.

HuR is expressed in most populations of sensory neurons and nerve fibers. HuR was highly expressed in the nucleus of sensory neurons. It was also present in the cytoplasm and in the sciatic nerve. A key question moving forward is if HuR localization is modulated by noxious cues in nociceptors. There are several pathways that could potentially affect HuR localization and function. Phosphorylation of HuR by p38 MAPK results in increased cytoplasmic retention and stabilization of mRNA targets (Lafarga et al., 2009). NGF stimulates p38 MAPK (Ji et al., 2002). The translational targets of p38 MAPK are largely unknown with the notable exception of TRPV1. Inhibition of p38MAPK diminishes inflammation-induced thermal hypersensitivity in rodents and neuropathic pain with an inflammatory component in humans (Melemedjian et al., 2010; Anand et al., 2011). Is HuR a mechanistically relevant target of p38 MAPK for pain? Although we do not know the answer, our HuR conditional knock-out model provides a means to test this hypothesis.

Sensory neurons are pivotal to nociceptive sensitization. Local protein synthesis in either the terminals of nociceptors or distal axons appears to be essential for long-lived changes in their excitability (Obara et al., 2012). These changes are believed to underlie hypersensitivity to mechanical and thermal cues, a hallmark of acute and chronic pain. Despite the importance of maladaptive nociceptive plasticity, the underlying mechanisms are

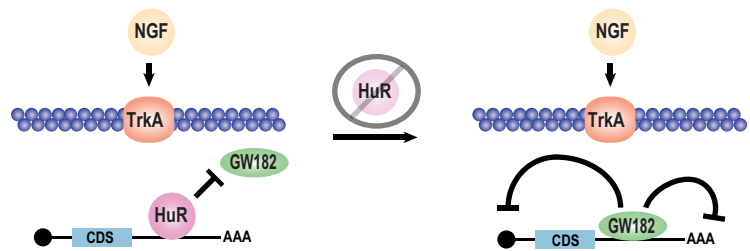


Figure 6. A model for the mechanism of HuR in sensory neurons. HuR is found near TrkA. We propose that one function of HuR is to prevent the association of repressive factors such as DCP1a and GW182 with receptor proximal transcripts. Deletion of HuR results in increased amounts of repressive factors with TrkA and may trigger precocious repression or destabilization of a subset of receptor proximal mRNAs.

poorly understood. Structural features ubiquitously present on mRNA, specifically the m7G cap and poly(A) tail, appear to be critical (Ferrari et al., 2013; Moy et al., 2017; Barragán-Iglesias et al., 2018; Ashraf et al., 2019). Astonishingly little is known about post-transcriptional regulatory factors in this context. An exception is the cytoplasmic polyadenylation element binding protein (CPEB1). It is involved in stimulation of translation via recognition of *cis*-acting elements situated in the 3'UTR and has been linked to nociceptive pain (Bogen et al., 2012). Another is DICER, a dsRNA ribonuclease that is required for the maturation of most miRNAs. Loss of DICER results in diminished mechanical sensitivity to inflammatory insults (Zhao et al., 2010). The data we present on HuR contributes to a growing body of literature that identifies factors involved in mRNA control as important for pain signaling (Wistrom et al., 2022). An exciting area of pharmacology is the growth of compounds that act on RNA-binding proteins. This work capitalizes on one such compound and underscores the potential utility in disrupting RNA-binding proteins for reduction of inflammation-associated pain (Wu et al., 2015; de la Peña and Campbell, 2018). We also identify HuR as important for the activity of hiPSC-derived nociceptors. This is, to the best of our knowledge, the first example of an RNA-binding protein that regulates nociceptor activity in humans. A key question moving forward is understanding if the targets of HuR are similarly maintained.

A major feature of local protein synthesis is engagement of receptors by extracellular cues and subsequent stimulation of translation. Intriguingly, there is significant variation in the identity of RNA-binding proteins near different receptor types (Koppers et al., 2019). These couplings might provide a means to localize specific populations of mRNA to the sites where they will eventually be translated. Another potential outcome from variation in receptor-RNA-binding protein interactions is precise regional control of mRNA stability and translational efficiency. We found that deletion of HuR from sensory neurons led to an increase in GW182 and Dcp1 near the NGF receptor, TrkA (Wiesmann et al., 1999). We propose a model for HuR function where it protects pronociceptive mRNAs near sites of local translation (Fig. 6). In the absence of HuR, abnormal repression may prevent nociceptive plasticity and abnormal behavioral responses. This raises the logical question of what are the relevant transcripts? HuR binds ~3500 targets in HeLa cells (Lebedeva et al., 2011). A major challenge moving forward will be mapping these interactions in nociceptors with the ultimate goal of understanding which are biologically important.

In summary, we have identified a conserved RNA-binding protein that plays an important role in nociceptor activity and

pain-associated behavioral responses. Given the paucity of information regarding the identity and function of RNA-binding proteins in nociceptive neurons, this work contributes new insights into the complex and vital roles of post-transcriptional control in pain signaling.

References

- Abdelmohsen K, Pullmann R Jr, Lal A, Kim HH, Galban S, Yang X, Blethor JD, Walker M, Shubert J, Gillespie DA, Furneaux H, Gorospe M (2007) Phosphorylation of HuR by Chk2 regulates SIRT1 expression. *Molecular cell* 25:543–557.
- Ahmed Z, Shaw G, Sharma VP, Yang C, McGowan E, Dickson DW (2007) Actin-binding proteins coronin-1a and IBA-1 are effective microglial markers for immunohistochemistry. *J Histochem Cytochem* 55:687–700.
- Al-Khalaf HH, Aboessekhra A (2014) ATR controls the UV-related upregulation of the CDKN1A mRNA in a Cdk1/HuR-dependent manner. *Mol Carcinog* 53:979–987.
- Anand P, Shenoy R, Palmer JE, Baines AJ, Robert YK Lai, Robertson J, Bird N, Ostenfeld T, Chizh BA (2011) Clinical trial of the P38 MAP kinase inhibitor diltiazem in neuropathic pain following nerve injury. *Eur J Pain* 15:1040–1048.
- Ashraf S, Radhi M, Gowler P, Burston JJ, Gandhi RD, Thorn GJ, Piccinini AM, Walsh DA, Chapman V, de Moor CH (2019) The polyadenylation inhibitor cordycepin reduces pain, inflammation and joint pathology in rodent models of osteoarthritis. *Sci Rep* 9:4696.
- Bailey TL, Elkan C, Hunter L, Searls D, Shavlik J (1995) Unsupervised learning of multiple motifs in biopolymers using expectation maximization. *Mach Learn* 21:51–80.
- Bailey TL, Johnson J, Grant CE, Noble WS (2015) The MEME Suite. *Nucleic Acids Res* 43:W39–W49.
- Barker PA, Patrick M, Lars A-N, Lars V, Tive L (2020) Nerve growth factor signaling and its contribution to pain. *J Pain Res* 13:1223–1241.
- Barragán-Iglesias P, Lou T-F, Bhat VD, Megat S, Burton MD, Price TJ, Campbell ZT (2018) Inhibition of poly(A)-binding protein with a synthetic RNA mimic reduces pain sensitization in mice. *Nat Commun* 9:10.
- Barragán-Iglesias P, Kunder N, Wangzhou A, Black B, Ray PR, Lou T-F, Bryan de la Peña J, Atmaramani R, Shukla T, Pancrazio JJ, Price TJ, Campbell ZT (2021) A peptide encoded within a 5' untranslated region promotes pain sensitization in mice. *Pain* 162:1864–1875.
- Behm-Ansmant I, Rehwinkel J, Doerks T, Stark A, Bork P, Izaurralde E (2006) mRNA degradation by MiRNAs and GW182 requires both CCR4:NOT deadenylase and DCP1:DCP2 decapping complexes. *Genes Dev* 20:1885–1898.
- Black BJ, Atmaramani R, Kumaraju R, Plagens S, Romero-Ortega M, Dussor G, Price TJ, Campbell ZT, Pancrazio JJ (2018) Cellular and molecular properties of neurons: adult mouse sensory neurons on microelectrode arrays exhibit increased spontaneous and stimulus-evoked activity in the presence of interleukin-6. *J Neurophysiol* 120:1374–1385.
- Black BJ, Atmaramani R, Plagens S, Campbell ZT, Dussor G, Price TJ, Pancrazio JJ (2019) Emerging neurotechnology for antinociceptive mechanisms and therapeutics discovery. *Biosens Bioelectron* 126:679–689.
- Bogen O, Alessandri-Haber N, Chu C, Gear RW, Levine JD (2012) Generation of a pain memory in the primary afferent nociceptor triggered by PKC ϵ activation of CPEB. *J Neurosci* 32:2018–2026.
- Borgonetti V, Galeotti N (2021) Intranasal delivery of an antisense oligonucleotide to the RNA-binding protein HuR relieves nerve injury-induced neuropathic pain. *Pain* 162:1500–1510.
- Braun JE, Huntzinger E, Fauser M, Izaurralde E (2011) GW182 proteins directly recruit cytoplasmic deadenylase complexes to MiRNA targets. *Mol Cell* 44:120–133.
- Bullitt E (1990) Expression of c-fos-like protein as a marker for neuronal activity following noxious stimulation in the rat. *J Comp Neurol* 296:517–530.
- Campbell ZT, Bhimsaria D, Valley CT, Rodriguez-Martinez JA, Menichelli E, Williamson JR, Ansari AZ, Wickens M (2012) Cooperativity in RNA-protein interactions: global analysis of RNA binding specificity. *Cell Rep* 1:570–581.
- Campbell ZT, Valley CT, Wickens M (2014) A protein-RNA specificity code enables targeted activation of an endogenous human transcript. *Nat Struct Mol Biol* 21:732–738.
- Chaplan SR, Bach FW, Pogrel JW, Chung JM, Yaksh TL (1994) Quantitative assessment of tactile allodynia in the rat paw. *J Neurosci Methods* 53:55–63.
- Chase R, Bryan de la Peña J, Smith PR, Lawson J, Lou T-F, Stanowick AD, Black BJ, Campbell ZT (2022) Global analyses of mRNA expression in human sensory neurons reveal EIF5A as a conserved target for inflammatory pain. *FASEB J* 36:e22422.
- Chekulaeva M, Mathys H, Zipprich JT, Attig J, Colic M, Parker R, Filipowicz W (2011) MiRNA repression involves GW182-mediated recruitment of CCR4-NOT through conserved W-containing motifs. *Nat Struct Mol Biol* 18:1218–1226.
- Costa-Mattioli M, Sossin WS, Klann E, Sonenberg N (2009) Translational control of long-lasting synaptic plasticity and memory. *Neuron* 61:10–26.
- Crawford LK, Caterina MJ (2020) Functional anatomy of the sensory nervous system: updates from the neuroscience bench. *Toxicol Pathol* 48:174–189.
- Curtis MJ, Alexander S, Cirino G, Docherty JR, George CH, Gienbycz MA, Hoyer D, Insel PA, Izzo AA, Ji Y, MacEwan DJ, Sobey CG, Stanford SC, Teixeira MM, Wonnacott S, Ahluwalia A (2018) Experimental design and analysis and their reporting II: updated and simplified guidance for authors and peer reviewers. *Br J Pharmacol* 175:987–993.
- de la Peña JB, Campbell ZT (2018) RNA-binding proteins as targets for pain therapeutics. *Neurobiol Pain* 4:2–7.
- de la Peña JB, Barragán-Iglesias P, Lou T-F, Kunder N, Loerch S, Shukla T, Basavarajappa L, Song J, James DN, Megat S, Moy JK, Wangzhou A, Ray PR, Hoyt K, Steward O, Price TJ, Shepherd J, Campbell ZT (2021a) Intercellular arc signaling regulates vasodilation. *J Neurosci* 41:7712–7726.
- de la Peña JB, Kunder N, Lou T-F, Chase R, Stanowick A, Barragán-Iglesias P, Pancrazio JJ, Campbell ZT (2021b) A role for translational regulation by S6 kinase and a downstream target in inflammatory pain. *Br J Pharmacol* 178:4675–4690.
- de la Peña JBI, Song JJ, Campbell ZT (2019) RNA control in pain: blame it on the messenger. *Wiley Interdiscip Rev RNA* 10:e1546.
- Deshmukh V, Prasoon P, Ray S (2016) Role of peripherin in defining specific populations of cell bodies in the dorsal root ganglia. *Int J Med Sci Public Health* 5:1656.
- Diaz-Muñoz MD, Bell SE, Fairfax K, Monzon-Casanova E, Cunningham AF, Gonzalez-Porta M, Andrews SR, Bunik VI, Zarnack K, Curk T, Heggermont WA, Heymans S, Gibson GE, Kontoyiannis DL, Ule J, Turner M (2015) The RNA-binding protein HuR (Elavl1) is essential for the B cell antibody response. *Nat Immunol* 16:415–425.
- Ferrari LF, Bogen O, Chu C, Levine JD (2013) Peripheral administration of translation inhibitors reverses increased hyperalgesia in a model of chronic pain in the rat. *J Pain* 14: 731–738.
- Ferrari LF, Araldi D, Levine JD (2015) Distinct terminal and cell body mechanisms in the nociceptor mediate hyperalgesic priming. *J Neurosci* 35:6107–6116.
- Filippova N, Yang X, King P, Nabors LB (2012) Phosphoregulation of the RNA-binding protein Hu antigen R (HuR) by Cdk5 affects centrosome function. *J Biol Chem* 287:32277–32287.
- Fong SW, Lin H-C, Wu M-F, Chen C-C, Huang Y-S (2016) CPEB3 deficiency elevates TRPV1 expression in dorsal root ganglia neurons to potentiate thermosensation. *PLoS One* 11:e0148491.
- Ghosh M, Aguila HL, Michaud J, Ai Y, Wu MT, Hemmes A, Ristimaki A, Guo C, Furneaux H, Hla T (2009) Essential role of the RNA-binding protein HuR in progenitor cell survival in mice. *J Clin Invest* 119:3530–3543.
- Gibson DG, Young L, Yuan Chuang R, Venter JC, Hutchison CA, Smith HO (2009) Enzymatic assembly of DNA molecules up to several hundred kilobases. *Nat Methods* 6:343–345.
- He Z-X, Song H-F, Liu T-Y, Ma J, Xing Z-K, Yin Y-Y, Liu L, Zhang Y-N, Zhao Y-F, Yu H-L, He X-X, Guo W-X, Zhu X-J (2019) HuR in the medial prefrontal cortex is critical for stress-induced synaptic dysfunction and depressive-like symptoms in mice. *Cereb Cortex* 29:2737–2747.
- Hinman MN, Lou H (2008) Diverse molecular functions of Hu proteins. *Cell Mol Life Sci* 65:3168–3181.
- Hyeon HK, Kuwano Y, Srikantan S, Eun KL, Martindale JL, Gorospe M (2009) HuR recruits let-7/RISC to repress c-Myc expression. *Genes Dev* 23: 1743–1748.
- Iida T, Yi H, Liu S, Huang W, Kanda H, Lubarsky DA, Hao S (2016) Spinal CPEB-MtROS-CBP signaling pathway contributes to perineural HIV

- Gp120 with DdC-related neuropathic pain in rats. *Exp Neurol* 281:17–27.
- Ishikawa T, Miyagi M, Ohtori S, Aoki Y, Ozawa T, Doya H, Saito T, Moriya H, Takahashi K (2005) Characteristics of sensory DRG neurons innervating the lumbar facet joints in rats. *Eur Spine J* 14:559–564.
- Ji R-R, Samad TA, Jin S-X, Schmoll R, Woolf CJ (2002) P38 MAPK activation by NGF in primary sensory neurons after inflammation increases TRPV1 levels and maintains heat hyperalgesia. *Neuron* 36:57–68.
- Kandasamy R, Price TJ (2015) The pharmacology of nociceptor priming. *Handb Exp Pharmacol* 227:15–37.
- Kim AY, Tang Z, Liu Q, Patel KN, Maag D, Geng Y, Dong X (2008) Pirt, a phosphoinositide-binding protein, functions as a regulatory subunit of TRPV1. *Cell* 133:475–485.
- Kleggetveit IP, Namer B, Schmidt R, Helås T, Rückel M, Ørstavik K, Schmelz M, Jorum E (2012) High spontaneous activity of C-nociceptors in painful polyneuropathy. *Pain* 153:2040–2047.
- Koppers M, Cagnetta R, Shigeoka T, Wunderlich LC, Vallejo-Ramirez P, Qiaojin Lin J, Zhao S, Jakobs MA, Dwivedy A, Minett MS, Bellon A, Kaminski CF, Harris WA, Flanagan JG, Holt CE (2019) Receptor-specific interactome as a hub for rapid cue-induced selective translation in axons. *Elife* 8:e48718.
- Kumar R, Kumar Poria D, Ray PS (2021) RNA-binding proteins La and HuR cooperatively modulate translation repression of PDCD4 mRNA. *J Biol Chem* 296:100154.
- Kundu P, Fabian MR, Sonenberg N, Bhattacharyya SN, Filipowicz W (2012) HuR protein attenuates miRNA-mediated repression by promoting miRISC dissociation from the target RNA. *Nucleic Acids Res* 40:5088–5100.
- Lafarga V, Cuadrado A, Lopez de Silanes I, Bengoechea R, Fernandez-Capetillo O, Nebreda AR (2009) P38 mitogen-activated protein kinase- and HuR-dependent stabilization of P21Cip1 mRNA mediates the G1/S checkpoint. *Mol Cell Biol* 29:4341–4351.
- Lebedeva S, Jens M, Theil K, Schwanhäusser B, Selbach M, Landthaler M, Rajewsky N (2011) Transcriptome-wide analysis of regulatory interactions of the RNA-binding protein HuR. *Mol Cell* 43:340–352.
- LeGendre JB, Campbell ZT, Kroll-Conner P, Anderson P, Kimble J, Wickens M (2013) RNA targets and specificity of stauflin, a double-stranded RNA-binding protein in *Caenorhabditis elegans*. *J Biol Chem* 288:2532–2545.
- Loerch S, de La Peña JB, Song J, Pancrazio JJ, Price TJ, Campbell ZT (2018) Translational controls in pain. In: *The Oxford handbook of neuronal protein synthesis* (Sossin WA, ed), pp 427–449. New York: Oxford UP.
- López de Silanes I, Zhan M, Lal A, Yang X, Gorospe M (2004) Identification of a target RNA motif for RNA-binding protein HuR. *Proc Natl Acad Sci U S A* 101:2987–2992.
- Lou T-F, Weidmann CA, Killingsworth J, Tanaka Hall TM, Goldstrohm AC, Campbell ZT (2017) Integrated analysis of RNA-binding protein complexes using *in vitro* selection and high-throughput sequencing and sequence specificity landscapes (SEQRS). *Methods* 118–119:171–181.
- Lyford GL, Yamagata K, Kaufmann WE, Barnes CA, Sanders LK, Copeland NG, Gilbert DJ, Jenkins NA, Lanahan AA, Worley PF (1995) Arc, a growth factor and activity-regulated gene, encodes a novel cytoskeleton-associated protein that is enriched in neuronal dendrites. *Neuron* 14:433–445.
- Masuda K, Abdelmohsen K, Kim MM, Srikantan S, Lee EK, Tominaga K, Selimyan R, Martindale JL, Yang X, Lehrmann E, Zhang Y, Becker KG, Wang J-Y, Kim HH, Gorospe M (2011) Global dissociation of HuR-mRNA complexes promotes cell survival after ionizing radiation. *EMBO J* 30:1040–1053.
- Matoulova E, Michalova E, Vojtesek B, Hrstka R (2012) The role of the 3' untranslated region in post-transcriptional regulation of protein expression in mammalian cells. *RNA Biol* 9:563–576.
- Mazan-Mamczarz K, Galbán S, López de Silanes I, Martindale JL, Atasoy U, Keene JD, Gorospe M (2003) RNA-binding protein HuR enhances P53 translation in response to ultraviolet light irradiation. *Proc Natl Acad Sci U S A* 100:8354–8359.
- Melemedjian OK, Asiedu MN, Tillu D, Peebles KA, Yan J, Ertz N, Dussor GO, Price TJ (2010) IL-6- and NGF-induced rapid control of protein synthesis and nociceptive plasticity via convergent signaling to the EIF4F complex. *J Neurosci* 30:15113–15123.
- Minatohara K, Akiyoshi M, Okuno H (2015) Role of immediate-early genes in synaptic plasticity and neuronal ensembles underlying the memory trace. *Front Mol Neurosci* 8:78.
- Moy JK, Khoutorsky A, Asiedu MN, Black BJ, Kuhn JL, Barragán-Iglesias P, Megat S, Burton MD, Burgos-Vega CC, Melemedjian OK, Boitano S, Vagner J, Gkogkas CG, Pancrazio JJ, Mogil JS, Dussor G, Sonenberg N, Price TJ (2017) The MNK-EIF4E signaling axis contributes to injury-induced nociceptive plasticity and the development of chronic pain. *J Neurosci* 37:7481–7499.
- Mukherjee N, Corcoran DL, Nusbaum JD, Reid DW, Georgiev S, Hafner M, Ascano M, Tuschl T, Ohler U, Keene JD (2011) Integrative regulatory mapping indicates that the RNA-binding protein HuR couples Pre-mRNA processing and mRNA stability. *Mol Cell* 43:327–339.
- Nadar M, Yu Chan M, Shi W, Huang, Huang CC, Tseng JT, Tsai CH (2011) HuR binding to AU-rich elements present in the 3' untranslated region of classical swine fever virus. *Virology* 418:1–8.
- North RY, Odem MA, Li Y, Tatsui CE, Cassidy RM, Dougherty PM, Walters ET (2022) Electrophysiological alterations driving pain-associated spontaneous activity in human sensory neuron somata parallel alterations described in spontaneously active rodent nociceptors. *J Pain* 23:1343–1357.
- Obara I, Géranton SM, Hunt SP (2012) Axonal protein synthesis: a potential target for pain relief? *Curr Opin Pharmacol* 12:42–48.
- Osmá-García IC, Capitan-Sobrinho D, Mouysset M, Bell SE, Lebeurier M, Turner M, Diaz-Muñoz MD (2021) The RNA-binding protein HuR is required for maintenance of the germinal centre response. *Nat Commun* 12:1–17.
- Park S, Myszkowski DG, Yu M, Littler SJ, Laird-Offringa IA (2000) HuD RNA recognition motifs play distinct roles in the formation of a stable complex with AU-rich RNA. *Mol Cell Biol* 20:4765–4772.
- Peng SS, Chen CY, Xu N, Shyu AB (1998) RNA stabilization by the AU-rich element binding protein, HuR, an ELAV protein. *EMBO J* 17:3461–3470.
- Perry MJ, Lawson SN, Robertson J (1991) Neurofilament immunoreactivity in populations of rat primary afferent neurons: a quantitative study of phosphorylated and non-phosphorylated subunits. *J Neurocytol* 20:746–758.
- Price TJ, Rashid MH, Millicamps M, Sanoja R, Entrena JM, Cervero F (2007) Decreased nociceptive sensitization in mice lacking the fragile X mental retardation protein: role of mGluR1/5 and mTOR. *J Neurosci* 27:13958–13967.
- Qiu C, Bhat VD, Rajeev S, Zhang C, Lasley AE, Wine RN, Campbell ZT, Tanaka Hall TM (2019) A crystal structure of a collaborative RNA regulatory complex reveals mechanisms to refine target specificity. *Elife* 8:e48968.
- Ray D, Kazan H, Chan ET, Peña Castillo L, Chaudhry S, Talukder S, Blencowe BJ, Morris Q, Hughes TR (2009) Rapid and systematic analysis of the RNA recognition specificities of RNA-binding proteins. *Nat Biotechnol* 27:667–670.
- Reichling DB, Levine JD (2009) Critical role of nociceptor plasticity in chronic pain. *Trends Neurosci* 32:611–618.
- Sanna MD, Peroni D, Quattrone A, Ghelardini C, Galeotti N (2015) Spinal RyR2 pathway regulated by the RNA-binding protein HuD induces pain hypersensitivity in antiretroviral neuropathy. *Exp Neurol* 267:53–63.
- Sanna MD, Quattrone A, Galeotti N (2017) Silencing of the RNA-binding protein HuR attenuates hyperalgesia and motor disability in experimental autoimmune encephalomyelitis. *Neuropharmacology* 123:116–125.
- Sebba A (2021) Pain: a review of Interleukin-6 and its roles in the pain of rheumatoid arthritis. *Open Access Rheumatol* 13:31–43.
- Silverman JD, Kruger L (1990) Selective neuronal glycoconjugate expression in sensory and autonomic ganglia: relation of lectin reactivity to peptide and enzyme markers. *J Neurocytol* 19:789–801.
- Skliris A, Papadaki O, Kafasla P, Karakasioti I, Hazapis O, Reczko M, Grammenoudi S, Bauer J, Kontoyiannis DL (2015) Neuroprotection requires the functions of the RNA-binding protein HuR. *Cell Death Differ* 22:703–718.
- Söderberg O, Gullberg M, Jarvius M, Ridderstråle K, Leuchowius K-J, Jarvius J, Wester K, Hydbring P, Bahram F, Larsson L-G, Landegren U (2006) Direct observation of individual endogenous protein complexes *in situ* by proximity ligation. *Nat Methods* 3:995–1000.
- Sorge RE, Si Y, Norian LA, Guha A, Moore GE, Nabors LB, Filippova N, Yang X, Smith R, Chellappan R, King PH (2022) Inhibition of the RNA regulator HuR by SRI-42127 attenuates neuropathic pain after nerve injury through

- suppression of neuroinflammatory responses. *Neurotherapeutics*. Advance online publication. Retrieved October 20, 2022.
- Srikantan S, Gorospe M (2012) HuR function in disease. *Front Biosci (Landmark Ed)* 17:189–205.
- Steward O, Wallace CS, Lyford GL, Worley PF (1998) Synaptic activation causes the mRNA for the IEG Arc to localize selectively near activated postsynaptic sites on dendrites. *Neuron* 21:741–751.
- Stucky CL, Lewin GR (1999) Isolectin B(4)-positive and -negative nociceptors are functionally distinct. *J Neurosci* 19:6497–6505.
- Tiruchinapalli DM, Caron MG, Keene JD (2008) Activity-dependent expression of ELAV/Hu RBPs and neuronal MRNAs in seizure and cocaine brain. *J Neurochem* 107:1529–1543.
- Wang H, Tiedge H (2004) Translational control at the synapse. *Neuroscientist* 10:456–466.
- Wang Y, Li Y, Toth JI, Petroski MD, Zhang Z, Zhao JC (2014) N6-methyladenosine modification destabilizes developmental regulators in embryonic stem cells. *Nat Cell Biol* 16:191–198.
- Weidmann CA, Qiu C, Arvola RM, Lou T-F, Killingsworth J, Campbell ZT, Tanaka Hall TM, Goldstrohm AC (2016) *Drosophila* Nanos acts as a molecular clamp that modulates the RNA-binding and repression activities of Pumilio. *Elife* 5:e17096.
- Wistrom E, Chase R, Smith PR, Campbell ZT, Correspondence T, Campbell Z (2022) A compendium of validated pain genes. *WIREs Mech Dis* 27:e1570.
- Wiesmann C, Ultsch MH, Bass SH, de Vos AM (1999) Crystal structure of nerve growth factor in complex with the ligand-binding domain of the TrkA receptor. *Nature* 401:184–188.
- Wolfe MB, Schagat TL, Paulsen MT, Magnuson B, Ljungman Mats, Park D, Zhang CHI, Campbell ZT, Goldstrohm AC, Freddolino PL (2020) Principles of mRNA control by human PUM proteins elucidated from multimodal experiments and integrative data analysis. *RNA* 26:1680–1703.
- Wu X, Lan L, Wilson DM, Marquez RT, Tsao W-C, Gao P, Roy A, Turner BA, McDonald P, Tunge JA, Rogers SA, Dixon DA, Aubé J, Xu L (2015) Identification and validation of novel small molecule disruptors of HuR-MRNA interaction. *ACS Chem Biol* 10:1476–1484.
- Zhang J, Zhang L, Jiao H, Zhang Q, Zhang D, Lou D, Katz JL, Xu M (2006) c-Fos facilitates the acquisition and extinction of cocaine-induced persistent changes. *J Neurosci* 26:13287–13296.
- Zhao J, Lee M-C, Momin A, Cendan C-M, Shepherd ST, Baker MD, Asante C, Bee L, Bethry A, Perkins JR, Nassar MA, Abrahamsen B, Dickenson A, Cobb BS, Merckenschlager M, Wood JN (2010) Small RNAs control sodium channel expression, nociceptor excitability, and pain thresholds. *J Neurosci* 30:10860–10871.
- Zhou Q, Kunder N, de La Paz JA, Lasley AE, Bhat VD, Morcos F, Campbell ZT (2018) Global pairwise RNA interaction landscapes reveal core features of protein recognition. *Nat Commun* 9:1–10.